Cell Host & Microbe, Volume *23*

Supplemental Information

The Marburgvirus-Neutralizing Human Monoclonal Antibody MR191 Targets a Conserved Site to Block Virus Receptor Binding

Liam B. King, Marnie L. Fusco, Andrew I. Flyak, Philipp A. Ilinykh, Kai Huang, Bronwyn Gunn, Robert N. Kirchdoerfer, Kathryn M. Hastie, Amandeep K. Sangha, Jens Meiler, Galit Alter, Alexander Bukreyev, James E. Crowe Jr., and Erica Ollmann Saphire

Supplemental information

Supplemental Table 1. Crystallographic data collection and refinement statistics. Related to Figure 1.

RAVV GP-MR191	
Wavelength (Å)	1.033
Resolution range (Å)	46.17-3.17 (3.29-3.17)
Space Group	P 3 2 1
Unit Cell (a,b,c in Å; α,β,γ in °)	a = 133.8, b = 133.8, c = 150.9 α = 90, β = 90, γ =120
Total reflections	296,807 (30,602)
Unique reflections	26,795 (2,652)
Multiplicity	11.0 (11.5)
Completeness (%)	99.28 (98.38)
Mean I/σ(I)	12.4 (1.3)
Wilson B-factor	98.1
R-merge	0.16 (2.02)
R-measured	0.17
CC(1/2)	0.998 (0.683)
CC*	1 (0.901)
Reflections used for R-free	1,360
R-work	0.263 (0.423)
R-free	0.291 (0.405)
Number of non-hydrogen atoms	5,687
Macromolecule atoms	5,559
Glycan atoms	128
Water	0
Protein residues	729
RMS (bonds)	0.012
RMS (angles)	1.52
Ramachandran favored (%)	95.0
Ramachandran allowed (%)	5.0
Ramachandran outliers (%)	0.0
Clashscore	6.1
Average B-factor	107.8
Macromolecules	107.4
Glycans	126.9

Supplemental Table 2. Sequencing of antibody CDRs. Relating to Figures 2, 3, and 5.

Heavy Chain			
Residue	Sequence	Kabat	IMGT
CDR-H1			
G	26	26	27
V	27	27	28
S	28	28	29
I	29	29	30
S	30	30	33
D	31	31	34
N	32	32	35
S	33	33	36
Y	34	34	37
Y	35	35	38
CDR-H2			
T	52	50	55
I	53	51	56
S	54	52	57
Y	55	53	58
S	56	54	59
G	57	55	60
N	58	56	64
T	59	57	65
Y	60	58	66
Y	61	59	67
N	62	60	68
P	63	61	69
S	64	62	70
L	65	63	71
K	66	64	72
S	67	65	74
CDR-H3			
Q	100	95	107
R	101	96	108
I	102	97	109
V	103	98	110
S	104	99	111
G	105	100	111A
F	106	100A	111B
V	107	100B	111C
E	108	100C	112B
W	109	100D	112A
L	110	100E	112
S	111	100F	113
K	112	100G	114
F	113	100H	115
D	114	101	116
Y	115	102	117

Light Chain			
Residue	Sequence	Kabat	IMGT
CDR-L1			
T	23	24	24
G	24	25	25
S	25	26	26
S	26	27	27
S	27	27A	28
N	28	27B	29
I	29	27C	30
G	30	28	31
A	31	29	35
G	32	30	36
F	33	31	37
D	34	32	38
V	35	33	39
H	36	34	40
CDR-L2			
D	52	50	56
N	53	51	57
N	54	52	65
N	55	53	66
R	56	54	67
P	57	55	68
S	58	56	69
CDR-L3			
Q	91	89	105
S	92	90	106
Y	93	91	107
D	94	92	108
T	95	93	109
S	96	94	110
L	97	95	112
S	98	95A	113
G	99	95B	114
P	100	95C	115
V	101	96	116
V	102	97	117
F	103	98	118
G	104	99	119
G	105	100	120
G	106	101	121
T	107	102	122
K	108	103	123
L	109	104	124
T	110	105	125
V	111	106	126
L	112	107	127

Supplemental Figure 1. Fc-mediated innate immune effector functions. Related to Figure 4.

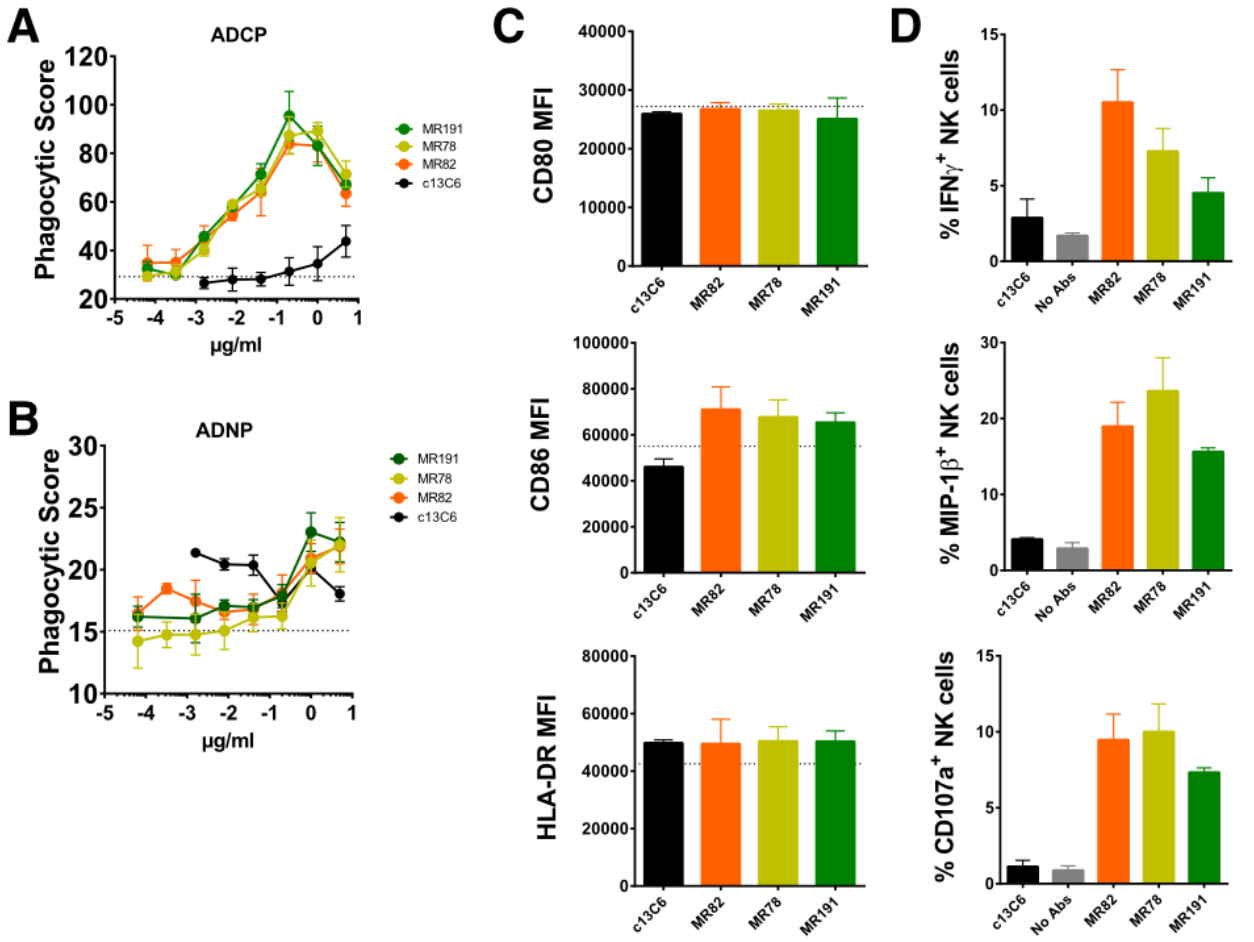

MR78, MR82 and MR191 were evaluated for induction of antibody-dependent phagocytosis of RAVV GP-coated beads by human monocytes **(A)**, neutrophils **(B)**, or monocyte-derived dendritic cells **(C)**. Activation of monocyte-derived dendritic cells following phagocytosis was determined by upregulation of HLA-DR, CD80, and CD86. Antibody-dependent activation of human NK cells was determined by degranulation as marked by expression of CD107a, and production of IFNγ and MIP-1β. Dashed line represents the levels of the no-antibody control. MR191, which demonstrated complete protection of both nonhuman primates and guinea pigs (Mire *et al.,* 2017), is colored green. MR78, which demonstrated partial protection of guinea pigs, is colored yellow. MR82, which failed to protect guinea pigs, is colored orange. Error bars indicate standard deviations.

Supplemental Figure 2. Disordered glycan cap. Related to Figure 2.

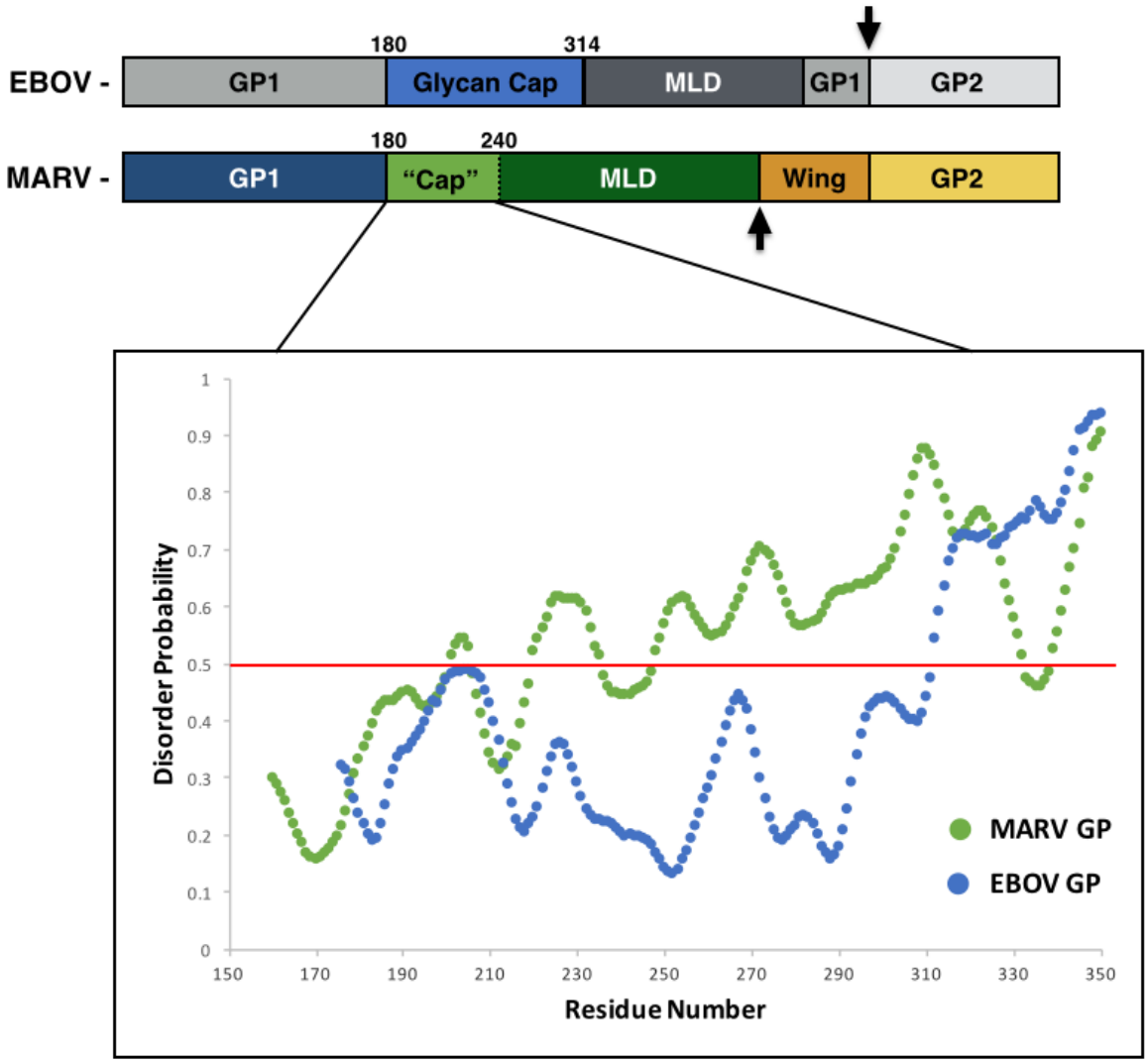

A schematic of EBOV GP is shown at top and MARV GP below, with arrows indicating the respective furin cleavage sites. The mucin-like domain (MLD) is disordered in both EBOV and MARV. The "cap" in MARV GP is a region containing residues that are equivalent in primary sequence *location* to the glycan cap in EBOV GP, but the residues in those positions bear little homology to those in EBOV. Below, predicted disorder of residues in the glycan cap of EBOV (blue) or equivalent residues in MARV (green) calculated using PrDOS software (Ishida and Kinoshita, 2007) is shown. Residues shown above the red line are predicted to be disordered. Graph shows greater predicted disorder within the MARV "cap" region.

Supplemental Figure 3. Supplemental mutagenesis of MR191 and RAVV GP. Related to Figure 3.

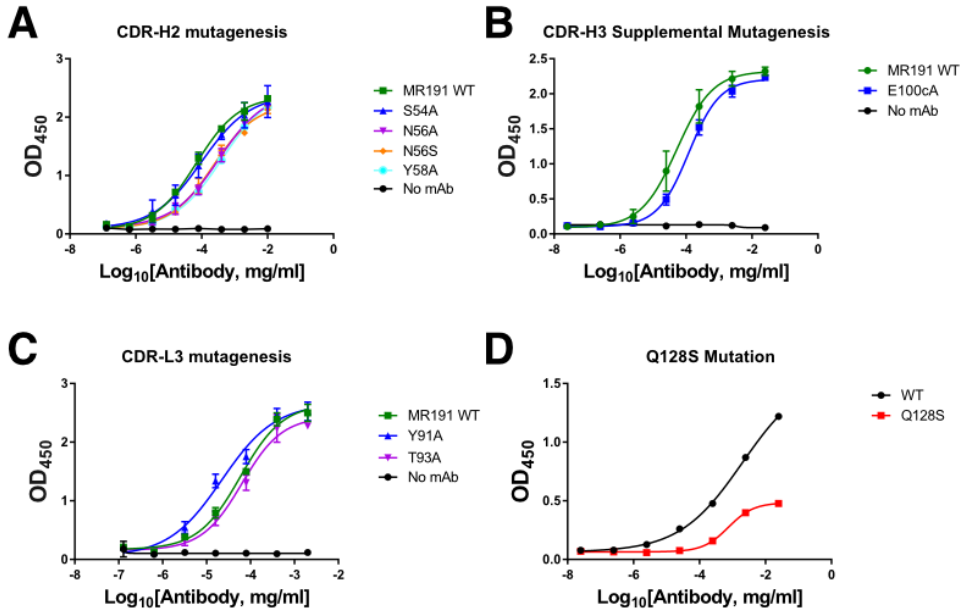

MR191 IgG1 antibodies were mutated in their CDR H2 or L3 and tested by ELISA for binding to RAVV GP. Antibodies mutated in these regions did not demonstrate significant differences in binding. Error bars indicate standard deviations.

Supplemental Figure 4. Rosetta comparative model. Related to Figure 1.

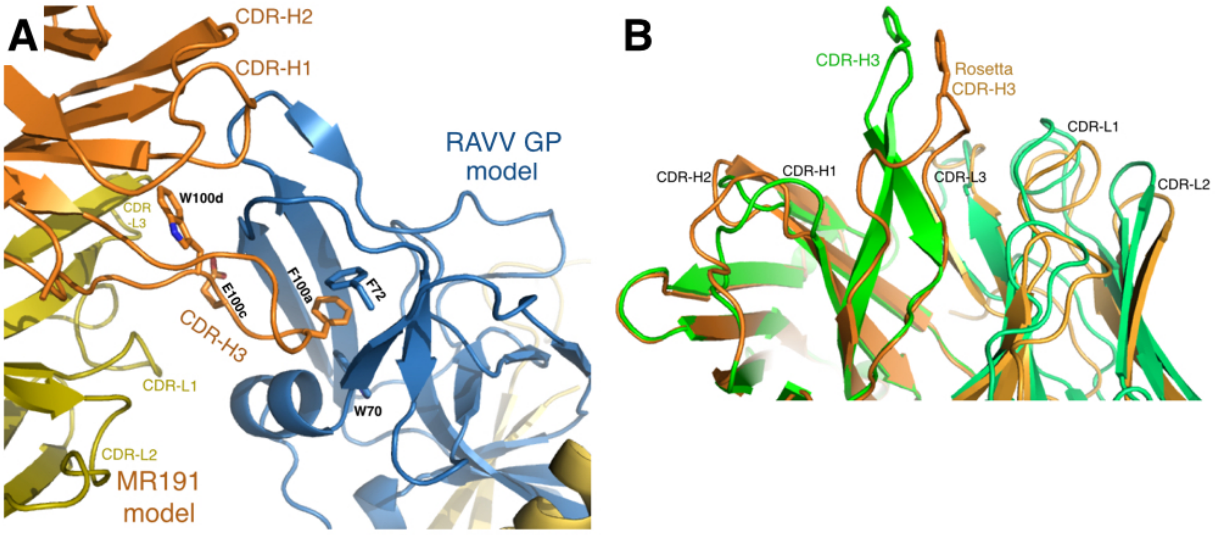

(A) Rosetta modeling of binding interaction between MR191 (orange) and RAVV GP (blue and gold). **(B)** The Fv region of MR191 was modeled from experimental crystallographic data (green) and Rosetta comparative modeling (orange). Several differences can be seen, most notably in the trajectories of CDR H2, H3, and L3.

Supplemental Figure 5. RAVV and EBOV "wing" region comparison. Related to Figure 2.

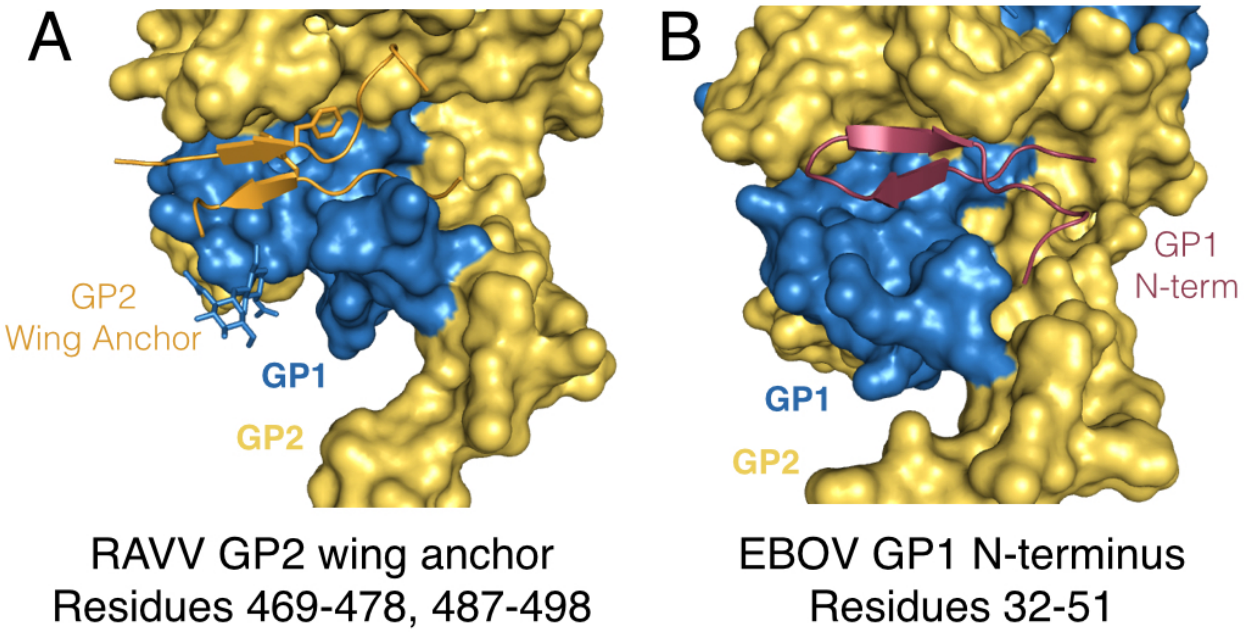

Comparison of RAVV GP and EBOV GP in the wing anchor region. The RAVV GP wing anchor (orange) binds between GP1 (blue) and GP2 (gold). In contrast, in EBOV, this space is occupied by the N terminus of GP1 (red). Despite different sequences of the RAVV GP2 wing and EBOV GP1 N terminus, both form antiparallel beta strands in this location.